(Received 10 November 2025, Accepted 28 November 2025, Scheduled 14 January 2026)

A Wearable CPW-Fed Quad-Band-Notched Two-Port MIMO Antenna for IoT Applications

Jiali Wang[1], Chengzhu Du[1,*], Jun Chu[1], and Ruomeng Li[2]

[1] College of Electronics and Information Engineering, Shanghai University of Electric Power, Shanghai 200090, China
[2] State Grid Jibei Electric Power Co., Ltd., Zhangjiakou Power Supply Company, Hebei, China

ABSTRACT: This paper introduces a wearable quad-band-notched two-port Multiple Input Multiple Output (MIMO) antenna with a coplanar waveguide (CPW)-fed for 5G applications. The antenna uses a liquid crystal polymer (LCP) flexible substrate with dimensions of 30 mm × 54 mm × 0.1 mm. The proposed antenna achieves four notched bands by etching four C-shaped slots on the patch and introduces a fence structure in the middle to enhance the isolation between the antenna elements, which ultimately achieves a band coverage of 3.26–10.8 GHz, with the notched-band coverage of 4.0–4.57 GHz (C-band radar Note7), 4.8–5.0 GHz (N79 mobile), 5.62–6.0 GHz (WLAN downlink), and 8.08–8.79 GHz (ITU-R), peak gain of 6.9 dBi, radiation efficiency above 70%, and isolation greater than 20 dB. In addition, the important performance parameters of the designed MIMO antenna include envelope correlation coefficient (ECC), diversity gain (DG), channel capacity loss (CCL), and total active reflection coefficient (TARC). The antenna is subjected to bending and human body experiments, and all the results show that the antenna has the advantages of small size, multiple notched bands, and high isolation, which has a good prospect of application in the field of wearable antennas for the Internet of Things (IoT).

1. INTRODUCTION

With the increasing maturation of 5G technology, its information transmission efficiency and speed have been significantly enhanced, leading to widespread applications in people's daily lives and industrial sectors [1]. Antennas play an indispensable role in data communication as passive devices that transmit and receive electromagnetic waves in wireless communication systems. Wearable antenna is a hot research topic in recent years, which has to realize miniaturization, low profile, and reduce the impact of radiation on human health when it is integrated into human attire. Wearable antennas can be used in biomedicine [2], where they can be worn inside a patient's clothing to help remotely access the services of doctors and healthcare professionals; in health monitoring, where they can be embedded in people's clothing to establish health detection and remote localization; in sports and fitness [3], where the antenna can be placed on the ground to sense the time of the exercise, attached to the runner's clothes or shoes to remotely time; and they can be used in military equipment and many other fields.

Wearable antennas need to be flexible and easily commensurable so that they can be better worn on the human body. Many researchers have used different flexible materials to make wearable antennas [4–8], such as Kapton Polyimide [4], Taconic TLY 5 [5], Rogers RT 5880 [6], Jeans textile [7], and LCP [8], and compare the performance of the antennas under different materials.

Multiple input multiple output (MIMO) technology uses multiple antennas at both the transmitter and receiver to significantly enhance spectral efficiency and channel capacity. It mitigates multipath fading, lowers error rates, and improves communication reliability. Recently, extensive research has been conducted on flexible MIMO antennas [9–12, 15, 17, 23]. In [9, 10, 15] employing Rogers substrates with different specifications (dielectric constant, thickness), antennas designed with Rogers materials offer performance advantages of high performance, high stability, and high reliability. In [11], a 4-port MIMO antenna is proposed, and transparency and flexibility of the antenna are achieved by utilizing materials like polyethylene terephthalate (PET) and silver oxide. In [12], the antenna is designed on a polyimide substrate. Refs. [17] and [23] utilize liquid crystal polymer (LCP) substrates with a thickness of merely 0.1 mm, which exhibit excellent flexibility and demonstrate promising application potential in the field of wearable antennas for the IoT (Internet of Things).

To prevent wide-bandwidth antennas from being interfered by narrowband signals and to enable the transmission and reception of specific frequency band signals, many researchers have proposed antennas with band-rejection characteristics [13–22]. The most common method to achieve stopbands is slot etching, such as L-shaped, U-shaped, or C-shaped slots. In [13], a U-type slit is cut into the patch to produce the band-notch at C-band across 3.63–4.15 GHz. In [15], an antenna consists of a circular monopole with a split ring groove. The band rejection feature is achieved by placing a split-ring resonator (SRR) slot, etching it on a circular monopole, and etching a U-shaped slot on the strip line feed. The antenna in [22] achieves quad-band rejection characteristics by incorporating a complementary split-ring resonator structure on the patch, placing two C-shaped structures on both

* Corresponding author: Chengzhu Du (duchengzhu@163.com).

sides of the feed line, and introducing two L-shaped slots at the edges of the ground plane.

In this paper, a wearable four-notched-band binary MIMO antenna is proposed for IoT applications in the paper. The antenna is fed by a CPW (coplanar waveguide) feed and achieves ultra-wideband (UWB) operation from 3.26 to 10.8 GHz. In order to realize the notched bands for special frequencies, four C-shaped slots are etched in the patch, which realize the four notched bands of C-band radar (Note7), N79 (mobile), WLAN downlink, and ITU-R, respectively. This design enables the antenna to effectively avoid co-channel interference from existing wireless systems, ensuring communication reliability in complex medical monitoring and industrial IoT environments. The antenna employs a binary MIMO configuration where a central fence structure ensures inter-element isolation exceeding 20 dB across the entire operating band. The measured and simulated results demonstrates outstanding performance metrics: an envelope correlation coefficient (ECC) below 0.03, diversity gain (DG) approaching 10 dB, and channel capacity loss (CCL) under 0.4 bits/s/Hz. This capability strongly supports bandwidth-intensive scenarios such as augmented reality (AR)-assisted remote collaboration. Combined with its flexible structure and compact design, the antenna can be seamlessly integrated into wearable devices and various IoT terminals.

2. ANTENNA DESIGN

2.1. Single Element Antenna

Figure 1 illustrates the entire design steps to realize the final unit antenna. The antenna is fed by CPW feed, and ultra-wideband characteristics are achieved by cutting a triangular patch, then four C-shaped slots are etched on the patch to make the current flow on both sides of the slots and in the opposite directions, generating mutually canceling electric fields and limiting the radiation of electromagnetic waves at the corresponding frequency bands, thus realizing four-notched bands, respectively, of the C-band radar (Note7), N79 (mobile), WLAN downlink, and ITU-R. The antenna is made of flexible LCP substrate material with a dielectric constant of 2.9, loss angle tangent of 0.002, and thickness h of 0.1 mm. Through continuous analysis and optimization in the HFSS software, the final antenna length was determined to be 6 mm and the width to be 14 mm. The calculation formulas for the dimensions of the rectangular patch are as follows:

$$W_0 = \frac{2F}{\sqrt{1+\frac{2h}{\pi\varepsilon_{eff}F\left[\ln\left(\frac{F\pi}{2h}\right)+1.7726\right]}}} \tag{1}$$

$$F = \frac{8.791*10^9}{f_0\sqrt{\varepsilon_{eff}}} \tag{2}$$

$$\varepsilon_{eff} \approx \frac{(\varepsilon_r+1)}{2} \tag{3}$$

In Equations (1)–(3), W_0 is the width of the radiation patch, $f_0 = 7.5$ GHz the resonant frequency, ε_{eff} the dielectric constant of substrate, and h the thickness of the antenna. The lengths of the two C-shaped slits are equal to a half-wavelength resonator, which can be calculated as

$$\lambda = \frac{C}{2f_0\sqrt{\varepsilon_{eff}}} \tag{4}$$

In Equation (4), c is the speed of light in a vacuum. In Fig. 1 the feed line width wg is 1.8 mm, and the spacing w between the feed line and the ground plane $g1$ is 0.2 mm. Calculating according to the above formula, the characteristic impedance Z_0 of the antenna is 50 Ω. The characteristic impedance Z_0 of the antenna can be calculated according to [24].

Figure 2 illustrates the S_{11} curves for different stages of the unit antenna. In Ant 1, the shape of the radiation patch is rectangular, and S_{11} does not reach the ultra-wideband. On this basis, the rectangular patch is corner-cut to become Ant 2, at which S_{11} realizes a broadband of 2.8–10.28 GHz. Then by etching four C-shaped slots on the patch, the final antenna band covers 2.8–10.8 GHz, where notched bands are generated at 4.17–4.6 GHz (C-band Radar Note7), 4.75–5.0 GHz (N79 mobile), 5.44–6.0 GHz (WLAN downlink), and 8.05–8.6 GHz (ITU-R).

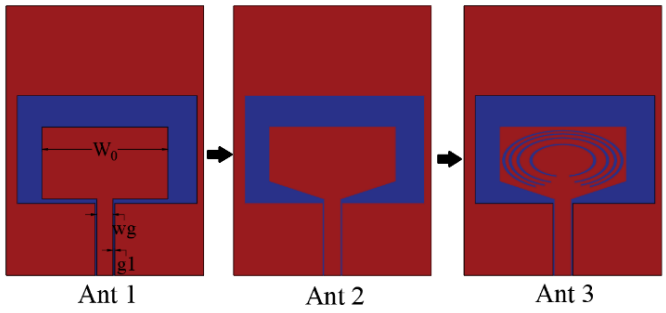

FIGURE 1. Unit antenna design steps.

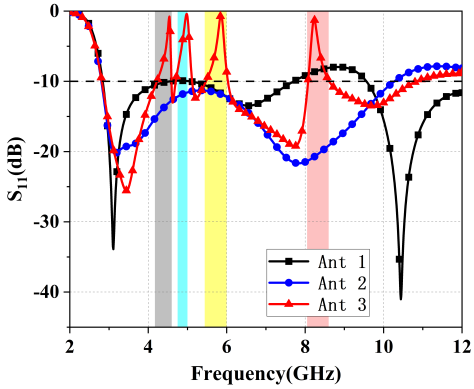

FIGURE 2. S_{11} for different stages of unit antenna.

2.2. Two-Element MIMO Antenna

Figure 3 shows the structural and processing physical drawings of the four-notched-band binary MIMO antenna. The two antenna units of the MIMO antenna are placed in parallel, and a fence structure is introduced in the center to enhance the isolation between the antenna elements. The final antenna size is

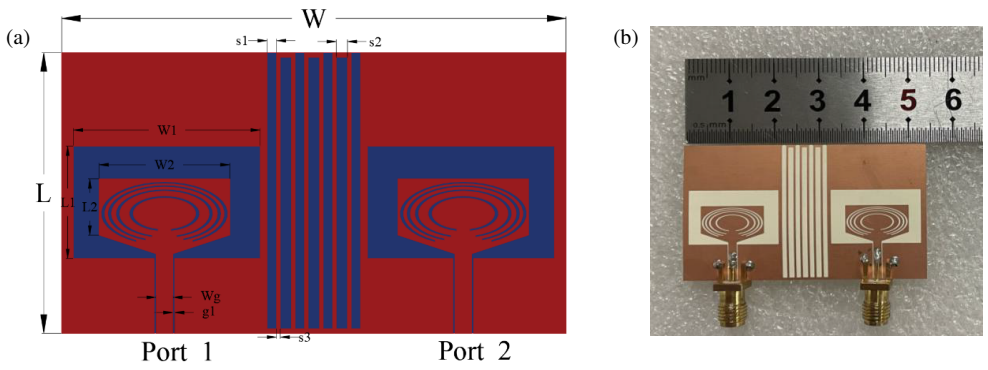

FIGURE 3. Structure and processed physical drawing of the presented antenna. (a) Antenna structure. (b) Fabricated antenna.

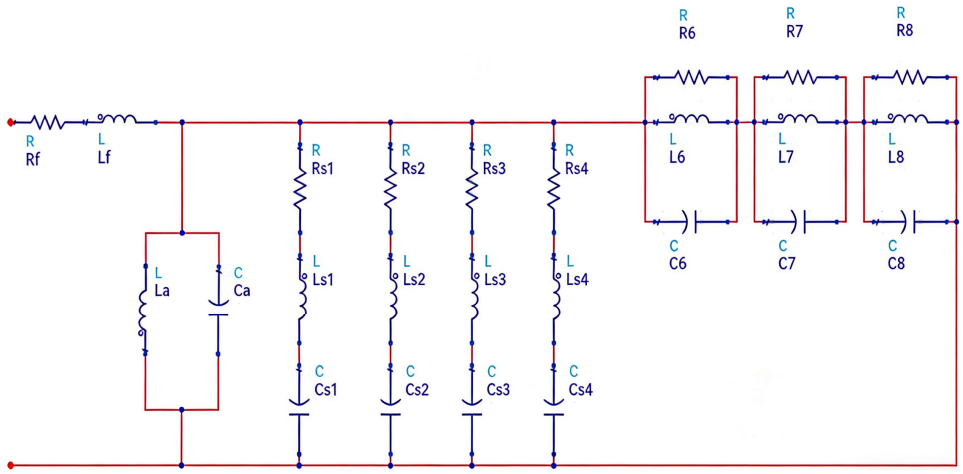

FIGURE 4. Equivalent circuit model of the proposed antenna.

TABLE 1. Simulated and optimized antenna geometry parameter values.

Parameters	L	W	$L1$	$W1$	$L2$	$W2$
Lengths (mm)	3	54	12	2	6	14
Parameters	$g1$	Wg	$s1$	$s2$	$s3$	/
Lengths (mm)	0.2	1.8	1	1.2	0.4	/

30 mm $*$ 54 mm $*$ 0.1 mm. The values of the simulated and optimized antenna geometric parameters are shown in Table 1.

Figure 4 illustrates the equivalent circuit model of the antenna configuration. This circuit model was developed using the Advanced Design System (ADS) simulation tool. A series of parallel R-L-C resonant circuits (R6-L6-C6, R7-L7-C7, and R8-L8-C8) are utilized to represent the equivalent circuit resonators of the main UWB antenna. The feed line is incorporated into the equivalent circuit and is represented by a series Rf-Lf to model the distributed elements of the antenna. The decoupling structure slot in the radiating patch is represented by an La-Ca resonator to broaden the impedance bandwidth. The arc-shaped slots are designed as series R-L-C circuits (RS1-LS1-CS1, RS2-LS2-CS2, RS3-LS3-CS3, and RS4-LS4-CS4). These components function as a short circuit at their resonant frequencies, causing most of the input power to be reflected back to the source. This effectively suppresses interference from the C-band Radar (Note7), N79 mobile, WLAN downlink, and ITU-R systems [25–27].

2.3. Decoupling Structure Analysis

Figure 5 shows the design process of the proposed antenna isolation structure. In Antenna 1, the two antenna units are placed horizontally without adding any isolation structure in between. In Antenna 2, the two antenna units are still placed horizontally, but a fence structure is introduced in the middle to connect the ground plates of the two antenna units, which reduces the inter-unit coupling and thus improves the isolation between the antenna units.

Figure 6 shows the S-parameter simulation schematics of Antenna 1 and Antenna 2. Among them, Fig. 6(a) shows the S_{11} simulation before and after adding the isolation structure, from which it can be seen that after adding the isolation structure, the low frequency is shifted to the right, but the overall impedance bandwidth does not change much, and the antenna after adding the isolation structure covers four notch bands, 4.0–4.57 GHz (C-band radar Note7), 4.8–5.0 GHz (N79 mobile), 5.62–6.0 GHz (WLAN downlink), and 8.08–8.79 GHz (ITU-R). Fig. 6(b) shows the change in the isolation degree of the antenna before and after increasing the isolation struc-

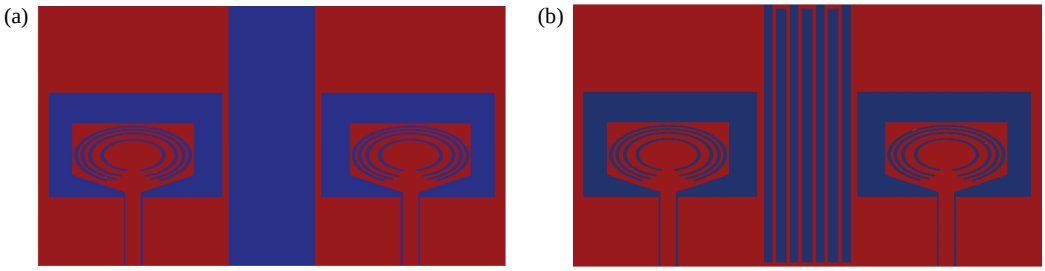

FIGURE 5. Antenna isolation structure design process. (a) Antenna 1, (b) Antenna 2.

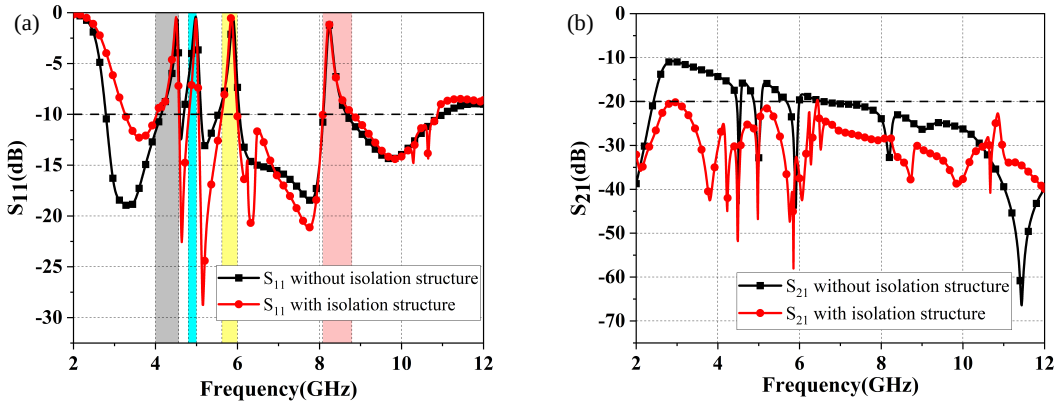

FIGURE 6. S-parameter simulation of Antenna 1 and Antenna 2, (a) S_{11}, (b) S_{21}.

ture, from which it can be seen that when the isolation structure is not increased, S_{21} is still unable to meet the requirements at the low frequency, whereas the isolation degree of the antenna is now less than -20 dB throughout the entire operating frequency band after the isolation structure is increased, which indicates that the isolation structure can improve the isolation degree of the antenna units and reduce the coupling between them.

Figure 7 shows the current distribution of the antenna at 4.5 GHz, 5.0 GHz, 5.9 GHz, and 8.2 GHz. From the figure, it can be seen that port 1 is excited while port 2 is terminated with a 50-ohm load, and the current is mainly distributed to the isolation structure, and the current flowing to port 2 is very little, which also further illustrates that the isolation structure can effectively reduce the coupling between the antenna units.

3. MEASURED RESULTS AND ANALYSIS

3.1. S-Parameters

Figure 8 shows the simulated and measured values of the S-parameters of the proposed wearable four-notched-bands binary MIMO antenna. Fig. 8(a) shows the simulated and measured values of the proposed antenna S_{11}, and it can be seen that although there is a little deviation between the measured and simulated curves at high frequencies, both the measured and simulated values cover the four notch bands of the C-band radar Note7, N79 mobile, WLAN downlink, and ITU-R, and thus, there is a better overall agreement between the two. Fig. 8(b) shows the simulated and measured values of the proposed antenna S_{21}, and it can be seen that both measured and simulated S_{21} are below -20 dB, which meets the requirements. The deviation between the measured and simulated S_{11} and S_{21} mainly comes from the errors in the antenna manufacturing process and the loss of the SMA connector.

3.2. Radiation Patterns

The antenna radiation pattern measurement of the far field is shown in Fig. 9. Fig. 10 illustrates the simulated and measured E-plane and H-plane normalized radiation direction plots at 4.7 GHz, 7.0 GHz, and 9.5 GHz. From the figure, it can be seen that the E-plane radiation patterns of the antenna are all in the shape of "8", indicating that the antenna has better directivity, and the H-plane radiation patterns are all in the shape of "O", indicating that the antenna has better omnidirectionality. The reason for the difference between the measured and simulated curves is mainly the errors during the testing process.

3.3. Gain and Efficiency

Figure 11 shows the simulated and measured gain and efficiency values of the proposed antenna at different frequencies in the operating band. In the operating band of the antenna, the measured gain is 4.5 dB when the frequency is 4.7 GHz, 6.1 dB when the frequency is 7.8 GHz, and 6.9 dB when the frequency is 9.5 GHz. Fig. 11(b) portrays that the actual efficiency of the antenna is approximately 70%. Then, because of environmental uncertainties, the measured performance in terms of gain and efficiency has some discrepancies compared to the calculated values.

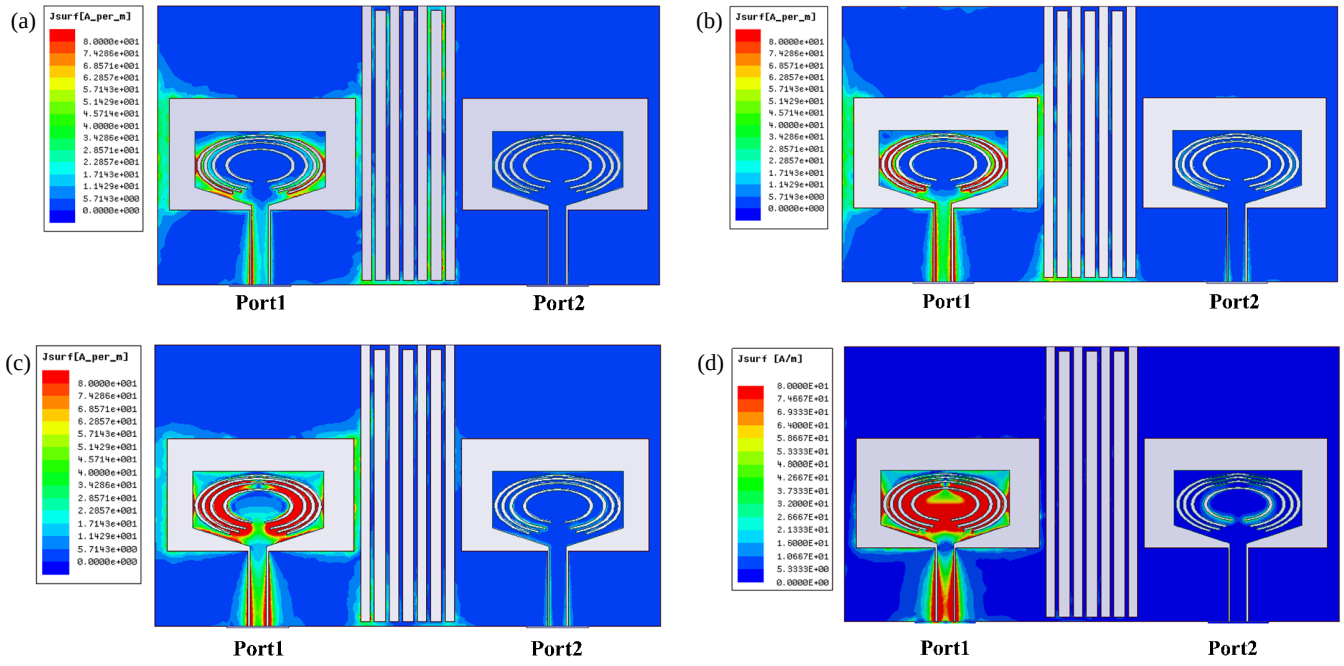

FIGURE 7. Current distribution of the antenna at different frequencies (a) at 4.5 GHz, (b) at 5.0 GHz, (c) at 5.9 GHz, (d) at 8.2 GHz.

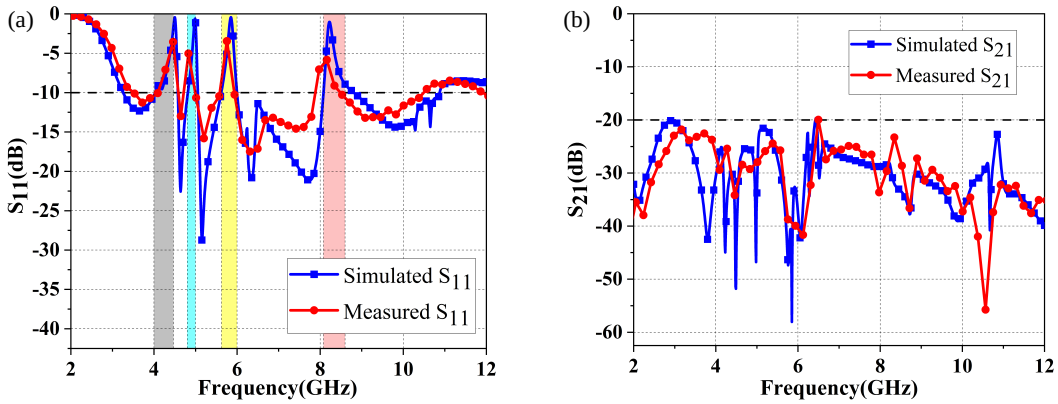

FIGURE 8. Antenna simulation and measured S-parameters, (a) S_{11}, (b) S_{21}.

FIGURE 9. Antenna radiation pattern measurement setup.

3.4. Diversity Performance

ECC, DG, CCL, and TARC are the metrics of the MIMO antenna to measure the diversity performance. ECC is defined as a performance metric of how isolated or correlated the communication channels are from each other. The smaller the value of ECC is, the less correlation is between two antennas, and the better the MIMO system is. The formulas for calculating ECC from far-field parameters and S-parameters can be obtained from [3]. The diversity performance of the antenna system is evaluated by the DG, which is a key parameter characterizing the diversity reception capability. To describe how fast the constant message transmission rate can attain in communication system, CCL is introduced [28]. CCL for MIMO antenna should maintain lower than 0.4 bits/s/Hz over working bands. TARC represents the effective operating bandwidth when multiple antennas are excited at the same time, and its value is lower than -10 dB in the frequency band, which indicates that the MIMO antenna system has low reflection loss

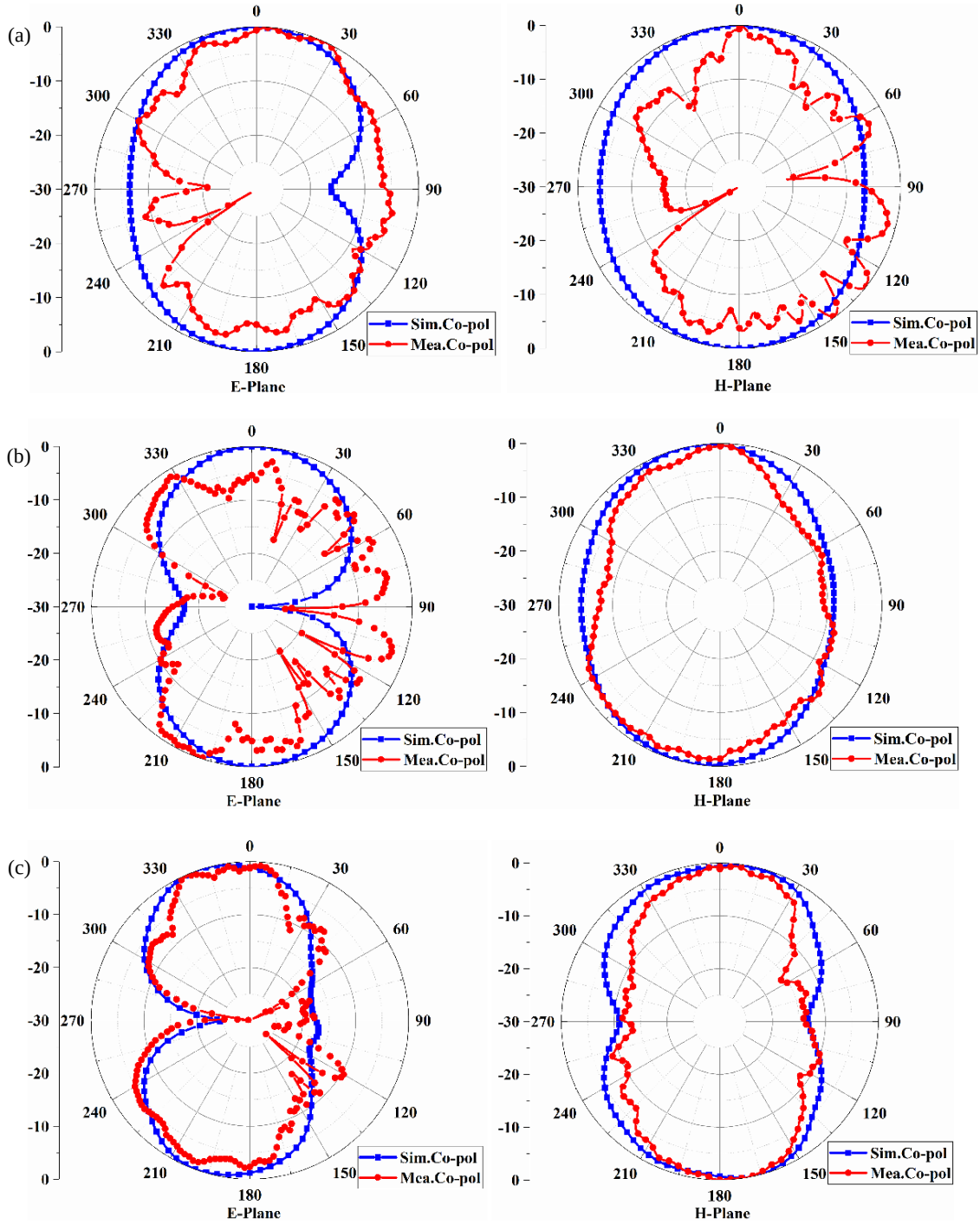

FIGURE 10. Radiation patterns in E-plane and H-plane (a) at 4.7 GHz, (b) at 7.0 GHz, (c) at 9.5 GHz.

and good phase stability, and can ensure reliable signal transmission.

The DG is calculated as follows (5):

$$\mathrm{DG} = 10\sqrt{1-(\mathrm{ECC})^2} \tag{5}$$

The TARC is calculated as follows (6):

$$\mathrm{TARC} = N^{-0.5}\sqrt{\sum_{i=1}^{N}\left|\sum_{k=1}^{N}\left|s_{ik}e^{j\theta k-1}\right|\right|^2} \tag{6}$$

Figure 12 shows the simulated and measured ECCs of the proposed antenna, and it can be seen that the measured ECC values are less than 0.03 in the operating band. Fig. 13 shows the simulated and measured DGs of the proposed antenna, and it can be seen that the measured DG values are all close to 10 dB in the operating band. In Fig. 14, the simulation CCL curves are presented, showing that the CCL meets the standard over operating bands. Fig. 15 shows the simulated value of the TARC of the proposed antenna, and it can be seen that when the θ-excitation phase angles are 0°, 60°, 120°, and 180°, the TARC values are all less than -10 dB in the operating fre-

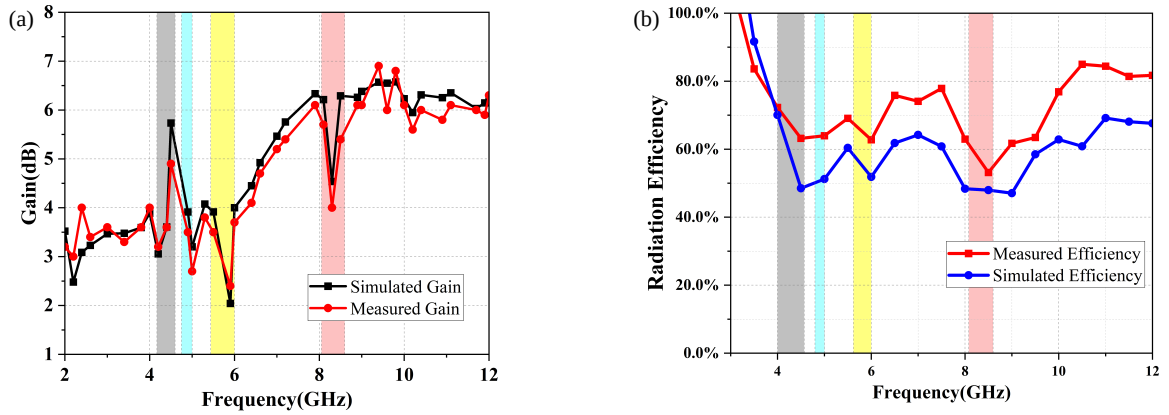

FIGURE 11. Antenna gain and efficiency. (a) Gain. (b) Radiation efficiency.

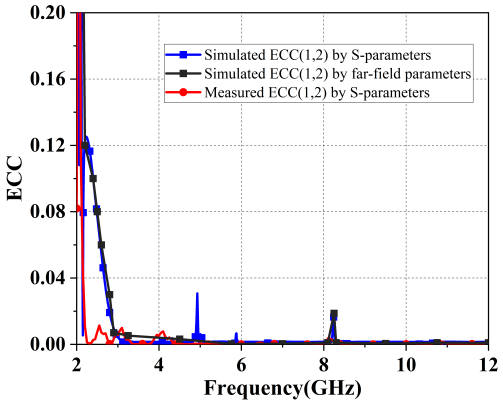

FIGURE 12. ECC of the presented antenna.

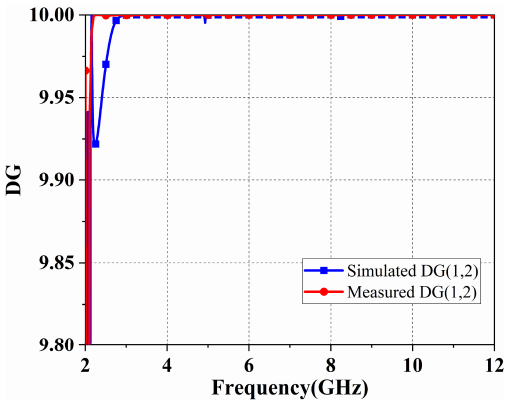

FIGURE 13. DG of the presented antenna.

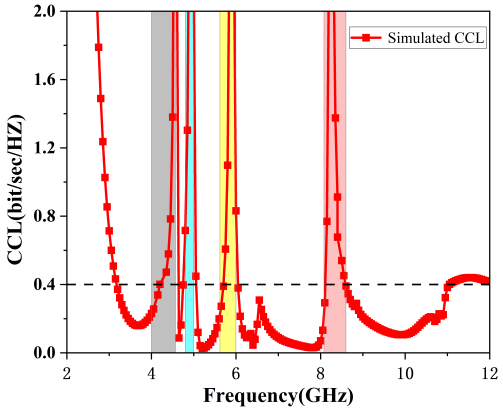

FIGURE 14. CCL of the presented antenna.

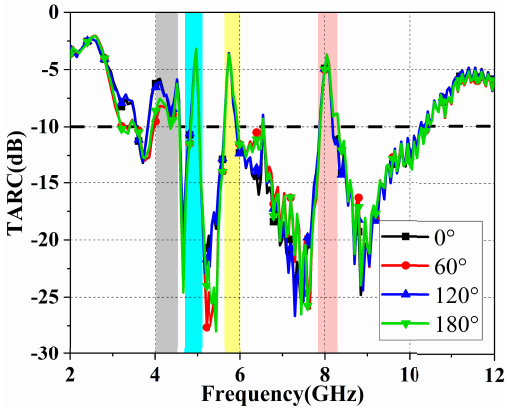

FIGURE 15. TARC of the presented antenna.

quency bands and greater than -10 dB in the four-notched-bands, which meets the requirements.

3.5. Flexibility Analysis

The antenna proposed in this paper is a flexible wearable antenna, so the effect of the degree of bending on this antenna needs to be investigated. The antennas were placed on the surface of plastic hollow cylinders with radii of 30 mm and 50 mm, and the S-parameters were measured and compared to those when they were not bent. Fig. 16 illustrates the S-parameters of the antenna for different bending states. From Fig. 16(b), it can be seen that when the antenna is placed on the surface of the plastic hollow cylinder with a radius of 30 mm, the antenna S_{11} fails to completely cover the four notch bands due to the large bending amplitude, and when the antenna is placed with a radius of 50 mm, the antenna S_{11} can cover the four notch bands of the C-band radar Note7, N79 mobile, WLAN downlink, and ITU-R. From Fig. 16(c), it can be seen that S_{21} of the antenna stays below -20 dB under different bending conditions, which meets the requirements. Thus, the antenna has an overall excellent performance under bending and can be applied in the wearable field.

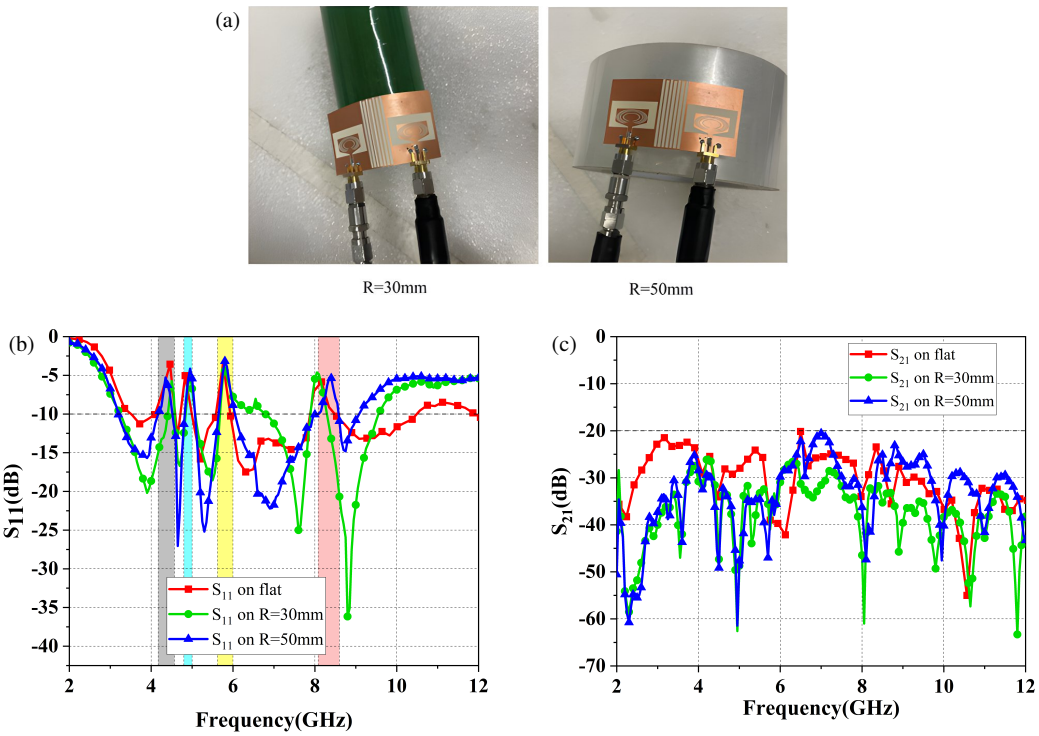

FIGURE 16. S-parameters of the antenna for different bending states. (a) Bending antenna, (b) S_{11}, (c) S_{21}.

3.6. Effects of Human Body

Specific Absorption Rate (SAR) refers to the power of electromagnetic wave absorbed or consumed by human tissues per unit mass per unit time. In wearable antenna, SAR value is used to measure the degree of impact of antenna radiant energy on human tissue in W/kg. The US federal standard requires that the SAR value should not exceed 1.6 W/kg, while the European federal standard requires that it should not exceed 2 W/kg. The SAR values of wearable antennas must meet these criteria to ensure safety when they are applied to the human body. Fig. 17 shows a simple human body model based on 10 g consisting of four layers, from the outside to the inside being skin, fat, muscle, and bone. Table 2 shows the electromagnetic characteristics of each layer of the human body model.

TABLE 2. Electromagnetic properties of various human tissues.

	Bone	Muscle	Fat	Skin
ε_r	18.49	52.67	5.27	37.95
σ (S/m)	0.82	1.77	0.11	1.49
Density (kg/m^3)	1008	1006	900	1001
Thickness (mm)	13	20	5	2

Table 3 shows the maximum SAR values of the proposed wearable antenna at different frequencies and different distances from the human body. H denotes the distance between the antenna and human model. According to the table, it can be concluded that the simulated SAR values under different conditions are better than the EU standard (2 W/kg/10 g).

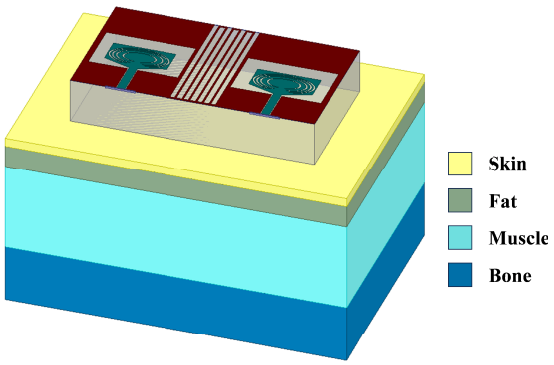

FIGURE 17. Antenna placed on the human body model.

TABLE 3. Maximum SAR values for different scenarios.

Central frequency (GHz)	H (mm)	SAR (W/kg/10 g)
4.7	8	1.0932
	10	0.8550
7.0	8	0.3622
	10	0.3275
9.5	8	0.2852
	10	0.2309

Figure 18 shows the measured values of the S-parameters of the antennas worn on the arm, chest, and thigh. From the figure, it can be seen that the antenna involved can cover the required frequency bands of different body parts, generate the required notch, and the isolation degree is less than -20 dB. Therefore, the antenna can work normally when it is placed on the body part.

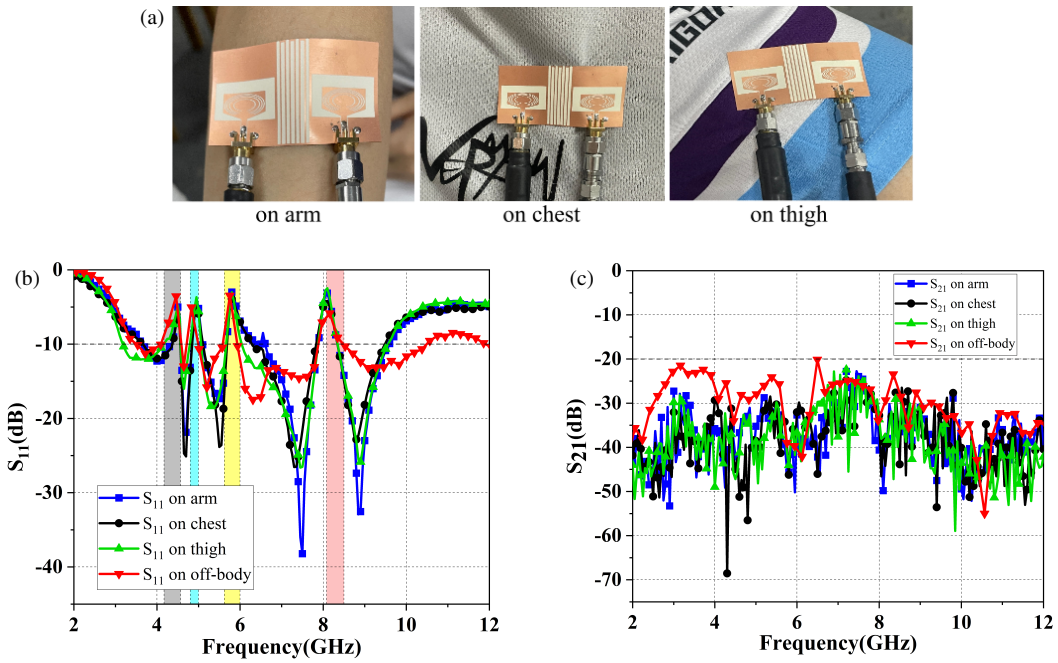

FIGURE 18. Measured S-parameters on different body parts. (a) Antenna on human tissue, (b) S_{11}, (c) S_{21}.

TABLE 4. Comparison of antenna performance.

Ref.	No. of ports	Antenna size (mm^3)	Substrate material	Bandwidth (GHz)	No. of notches	Isolation (dB)	ECC	DG
[17]	2	$30 * 56.5 * 0.1$	LCP (flexible)	2.4–11.3	1	< -23	< 0.008	> 9.998
[14]	2	$24 * 36 * 1.6$	FR4 (Non-flexible)	3.1–13.4	2	< -20	< 0.01	> 9.98
[5]	4	$54 * 54 * 1.52$	Taconic TLY 5 (Semi-flexible)	3.1–11.8	3	< -20	< 0.001	> 9.99
[15]	4	$48 * 48 * 1.6$	Rogers 5880 (Semi-flexible)	3–20	3	< -20	< 0.05	> 9.99
[18]	4	$65 * 65 * 0.8$	FR4 (Non-flexible)	2.51–11.07	3	< -21	< 0.005	> 9.998
[22]	2	$43 * 36 * 1.59$	/	1.4–25	4	< -15	< 0.005	/
Prop.	2	$30 \times 54 \times 0.1$	LCP (flexible)	3.26–10.8	4	< -20	< 0.03	> 9.99

4. PERFORMANCE COMPARISON

Table 4 lists the performance of the wearable four-notched-band binary MIMO antenna proposed in this paper compared to previous research works. In [14, 18], the antenna uses non-bendable rigid FR4 as the dielectric substrate material, which cannot be applied in the wearable field. Although flexible materials are used as the dielectric substrates in [5, 15, 17], the number of notched-bands is not as many as the proposed antenna, and the bending performance and isolation in [22] are inferior to that of the proposed antenna in this work. In summary, the proposed wearable four-notched-band binary MIMO antenna is characterized by small size, multiple notched bands, high isolation, and excellent co-conformal flexibility, which make it highly suitable for wearable IoT applications.

5. CONCLUSION

In this paper, a four-notched-band binary MIMO antenna is designed for wearable applications. The proposed antenna has four notched bands by etching four C-shaped slots on the patch, and a fence structure is introduced in the middle to improve the isolation between the elements. The MIMO antenna realizes the bandwidth of 3.26–10.8 GHz, and the four notched-bands are 4.0–4.57 GHz (C-band Radar Note7), 4.8–5.0 GHz (N79 mobile), 5.62–6.0 GHz (WLAN downlink), and 8.08–8.79 GHz (ITU-R). Its isolation is greater than 20 dB, its ECC value less than 0.03, DG close to 10, CCL below 0.4 bits/s/Hz, TARC lower than -10 dB in the frequency band, the maximum gain 6.9 dB, and radiation efficiency above 70%. The antenna shows good performance in bending tests. In human model simula-

tion, the antenna's SAR values are all below standard values under different conditions. The flexible MIMO antenna is suitable for wearable IoT applications, featuring multiple notched-bands, high isolation, small size, ease of conformal integration, and low SAR.

REFERENCES

[1] Desai, A., M. Palandoken, J. Kulkarni, G. Byun, and T. K. Nguyen, "Wideband flexible/transparent connected-ground MIMO antennas for sub-6 GHz 5G and WLAN applications," *IEEE Access*, Vol. 9, 147 003–147 015, 2021.

[2] Zhao, Z., C. Zhang, Z. Lu, H. Chu, S. Chen, M. Liu, and G. Li, "A miniaturized wearable antenna with five band-notched characteristics for medical applications," *IEEE Antennas and Wireless Propagation Letters*, Vol. 22, No. 6, 1246–1250, 2023.

[3] Zhang, J., C. Du, and R. Wang, "Design of a four-port flexible UWB-MIMO antenna with high isolation for wearable and IoT applications," *Micromachines*, Vol. 13, No. 12, 2141, 2022.

[4] Li, W., Y. Hei, P. M. Grubb, X. Shi, and R. T. Chen, "Compact inkjet-printed flexible MIMO antenna for UWB applications," *IEEE Access*, Vol. 6, 50 290–50 298, 2018.

[5] Abbas, A., N. Hussain, M. A. Sufian, W. A. Awan, J. Jung, S. M. Lee, and N. Kim, "Highly selective multiple-notched UWB-MIMO antenna with low correlation using an innovative parasitic decoupling structure," *Engineering Science and Technology, An International Journal*, Vol. 43, 101440, 2023.

[6] Sharma, M., "Design and analysis of MIMO antenna with high isolation and dual notched band characteristics for wireless applications," *Wireless Personal Communications*, Vol. 112, No. 3, 1587–1599, 2020.

[7] Biswas, A. K., S. Biswas, S. Haldar, and A. Nandi, "A highly decoupled flexible 4-element MIMO antenna with band notched characteristics for ultra wide-band wearable applications," *AEU — International Journal of Electronics and Communications*, Vol. 173, 154985, 2024.

[8] Wang, T.-S., C.-Z. Du, H.-F. Shu, and Z.-H. Yue, "A flexible UWB slot antenna with quad band-notched characteristics for wearable application," *Progress In Electromagnetics Research C*, Vol. 140, 127–134, 2024.

[9] Azimov, U. F., A. Abbas, S.-W. Park, N. Hussain, and N. Kim, "A 4-port flexible MIMO antenna with isolation enhancement for wireless IoT applications," *Heliyon*, Vol. 10, No. 11, e32216, 2024.

[10] Ibrahim, A. A., M. I. Ahmed, and M. F. Ahmed, "A systematic investigation of four ports MIMO antenna depending on flexible material for UWB networks," *Scientific Reports*, Vol. 12, No. 1, 14351, 2022.

[11] Desai, A., H.-T. Hsu, B. M. Yousef, A. M. Ameen, Y.-F. Tsao, and A. A. Ibrahim, "UWB connected ground transparent 4-port flexible MIMO antenna for IoT applications," *IEEE Internet of Things Journal*, Vol. 11, No. 7, 12 475–12 484, 2024.

[12] Rajesh, G. and R. Poonkuzhali, "Design and analysis of CPW fed ultrathin flexible MIMO antenna for UWB and X-band applications," *IEEE Access*, Vol. 12, 96 704–96 717, 2024.

[13] Devana, V. N. K. R., A. Beno, C. P. Devadoss, Y. Sukanya, C. V. R. Sankar, P. Balamuralikrishna, S. Chandrasekhar, and K. V. Babu, "A compact self isolated MIMO UWB antenna with band notched characteristics," *IETE Journal of Research*, Vol. 70, No. 8, 6677–6688, 2024.

[14] Rao, B. R., K. S. Chakradhar, and D. Nataraj, "Design, optimization and experimental verification of UWB-MIMO antenna with WLAN and complete X-band notched characteristics, checked with characteristic mode analysis (CMA)," *Analog Integrated Circuits and Signal Processing*, Vol. 115, No. 1, 139–158, 2023.

[15] Vanka, S. and C. Chandrasekhar, "A miniaturized-slotted planar MIMO antenna with switchable configuration for dual-/triple-band notches," *AIP Advances*, Vol. 14, No. 2, 025039, 2024.

[16] Tang, Z., J. Zhan, X. Wu, Z. Xi, L. Chen, and S. Hu, "Design of a compact UWB-MIMO antenna with high isolation and dual band-notched characteristics," *Journal of Electromagnetic Waves and Applications*, Vol. 34, No. 4, 500–513, 2020.

[17] Du, C. and G. Jin, "A compact CPW-fed band-notched UWB-MIMO flexible antenna for WBAN application," *Journal of Electromagnetic Waves and Applications*, Vol. 35, No. 8, 1046–1058, 2021.

[18] Rekha, V. S. D., P. Pardhasaradhi, B. T. P. Madhav, and Y. U. Devi, "Dual band notched orthogonal 4-element MIMO antenna with isolation for UWB applications," *IEEE Access*, Vol. 8, 145 871–145 880, 2020.

[19] Jayant, S. and G. Srivastava, "Close-packed quad-element triple-band-notched UWB MIMO antenna with upgrading capability," *IEEE Transactions on Antennas and Propagation*, Vol. 71, No. 1, 353–360, 2023.

[20] Du, C.-Z., Z.-P. Yang, H.-Y. Liu, and Y. Nie, "Four-element CPW-fed UWB MIMO slot antenna with high isolation and triple band-notched characteristics," *Progress In Electromagnetics Research C*, Vol. 116, 145–156, 2021.

[21] Benghanem, Y., A. Mansoul, and L. Mouffok, "A compact two-element MIMO antenna with high isolation and dual band-notched characteristics for UWB communication systems," *Wireless Personal Communications*, Vol. 136, No. 2, 1107–1126, 2024.

[22] Zhao, L., Y. Wang, C. Liu, D. Song, C. Hu, C. Li, H. Zhao, and Z. Wang, "Compact circular-shaped MIMO antenna covers UWB bandwidth with four frequently-used band-notched characteristics for multi-scenario applications," *IEEE Access*, Vol. 12, 32 762–32 771, 2024.

[23] Du, C., H. Liu, X. Wang, Y. Nie, and Z. Yang, "Compact CPW-fed triple-band MIMO antenna for wireless body area network based on flexible liquid crystal polymer," *Journal of Electromagnetic Waves and Applications*, Vol. 36, No. 10, 1436–1450, 2022.

[24] Lian, S., H. Sun, H. Zhang, D. Zhang, T. Liu, Z. Jin, and Y. Zheng, "Transparent and flexible fish-tail shaped antenna for ultra-wideband MIMO systems," *Flexible and Printed Electronics*, Vol. 9, No. 3, 035007, 2024.

[25] Santhakumar, G. and R. Muthukumar, "A novel compact flower shaped antenna array for sub-6 GHz and UWB applications," *Wireless Networks*, Vol. 31, 2925–2938, 2025.

[26] Paul, S., S. Rana, A. R. Azad, D. Nandi, and A. Mohan, "Compact planar UWB microstrip antenna with independently controllable dual notch bands," *ETRI Journal*, 2025.

[27] Hussain, M., W. A. Awan, A. Alwabli, A. Y. Jaffar, W. N. Eid, and A. A. Althuwayb, "A PIN diode-enabled compact size antenna for transition between UWB and notched UWB modes," *Arabian Journal for Science and Engineering*, Vol. 50, 17 759–17 768, 2025.

[28] Shome, P. P., T. Khan, A. A. Kishk, and Y. M. M. Antar, "Quad-element MIMO antenna system using half-cut miniaturized UWB antenna for IoT-based smart home digital entertainment network," *IEEE Internet of Things Journal*, Vol. 10, No. 20, 17 964–17 976, 2023.